Science Advances

AAAS

advances.sciencemag.org/cgi/content/full/3/12/e1701423/DC1

Supplementary Materials for

Compressive 3D ultrasound imaging using a single sensor

Pieter Kruizinga, Pim van der Meulen, Andrejs Fedjajevs, Frits Mastik, Geert Springeling, Nico de Jong, Johannes G. Bosch, Geert Leus

Published 8 December 2017, *Sci. Adv.* **3**, e1701423 (2017)
DOI: 10.1126/sciadv.1701423

The PDF file includes:

Other Supplementary Material for this manuscript includes the following:
(available at advances.sciencemag.org/cgi/content/full/3/12/e1701423/DC1)

- movie S1 (.mp4 format). A random delay coding mask breaks the phase uniformity of the ultrasound transmission to enable compressive imaging.
- movie S2 (.mp4 format). Compressive 3D ultrasound imaging using a single sensor.
- movie S3 (.mp4 format). Image reconstruction for a multisensor array and a single sensor with rotating coding mask.

Supplementary Materials

text S1. On the size of the system matrix H.

Standard measurement systems are designed to provide a large number of measurements, generally much larger than the number of unknowns (M >> N), while guaranteeing that the condition number of the system matrix **H** is small enough, such that the problem of estimating **v** from **u** (**u** = **Hv** + **n**) is a well-posed problem. In current ultrasound devices for instance, this can be done by transmitting a short pulse through the tissue as a spatial beam or plane wave (repeated for several spatial beams or plane waves), followed by high-rate sampling (above the Nyquist rate) at every sensor (see also Fig. 1a and b). In compressive sensing imaging devices, however, far fewer measurements are taken, thereby reducing the imaging time considerably. In such scenarios, the number of measurements is often smaller than the number of unknowns (M<=N); even when M is larger than N, the system matrix **H** is typically ill-conditioned in compressive ultrasound imaging. In our case M is typically much smaller (between 10 and 100 times) than N. These values are highly dependent on pulse bandwidth, pulse length after the coding mask, number of rotations, size of imaging volume, and pixel size. In our case M is much smaller than N (10:1 for Fig.6 (b and d) and 100:1 for Fig. 6 (f), thus we need to constrain the solution space using some prior information. We describe these in the Materials and Methods section.

We attribute the successful reconstructions with fewer measurements than pixels to the fact that the dependence between columns in **H** is typically very local in space. Keeping in mind that the pixel size can be chosen arbitrarily, consider a large pixel size such that **H** contains more measurements than unknowns. As a consequence, the system becomes over-determined, but the modelling error due to reflectors that lay in between pixel positions will be rather large. To reduce this type of error, one would like to increase the pixel density by adding columns to **H**, resulting in fewer measurements than unknowns. It is obvious that the columns of the pixels that were added will be highly correlated to neighbouring pixels. Consequently, the solution ambiguity related to an echo signal coming from that region will be locally restricted to that image region. Combined with techniques like Tikhonov regularization, the least squares estimator will still be able to allocate energy to the corresponding region. The reconstruction will not be exact, but the allocated energy will be in approximately the correct part of the image.

text S2. Comparison with multisensor array imaging.

The imaging technique we propose relies on the inversion of complicated wavefields, making it difficult to compare our technique one-to-one with conventional geometrical beamforming techniques. For instance, our transmit beam is deliberately chaotic, and we have no ability of focusing this beam, unlike with normal sensor arrays. However, in the context of imaging by inversion we are able to compare the proposed single sensor with coding mask with a multi-sensor array. To this end we have extended our simulation analysis as described in the Materials and Methods section to further understand the influence of adding more sensors and the use of rotations on the imaging performance. In short, **H** was computed as described in "Approximate model and Cramer-Rao lower bound" of the Materials and Methods section. We pre-defined an image **v** (schematic drawing of a Toucan, in a xy-plane at a depth of 12.7 mm) and computed **u** via **u** = **Hv + n**. We then compared the estimated image $\hat{\mathbf{v}}$ with the true image **v** by computing the normalized mean square error (nsme) ($\mathbf{nmse} = ||\mathbf{v} - \hat{\mathbf{v}}||_2^2 / ||\mathbf{v}||_2^2$). For this analysis we used

similar settings as were used for Fig. 5. We considered the same aperture and coding mask. For the case of the multi-sensor array we removed the coding mask and subdivided the aperture in multiple sensors and excited all sensor subdivisions simultaneously. We compared the nmse as a function of mask rotations and number of sensors. The idea is that every mask rotation provides one unique measurement that should be comparable with the number of spatial measurements that can be obtained with multiple sensors in an array. Since the degree of wavefield complexity largely depends on the available delays in the coding mask, we also vary the local mask thickness from 1 to 8 mm. The overall results of these simulations can be observed in fig. S1. Reconstruction examples can be seen in fig. S2 and movie S3.

text S3. On the relation to CS.

For the results in Fig. 6f we used a technique more related to common CS methods. Traditional CS techniques require that the image **v** is sparse in some domain which can be represented by a basis matrix **G**. The representation **w** of the image in this domain is computed as **w** = **Gv**, and assuming **G** is invertible, the measurement equation can instead be written as

$$\mathbf{u} = \mathbf{H}\mathbf{v} = \mathbf{H}\mathbf{G}^{-1}\mathbf{w}$$

and solved for **w**. If **w** is sufficiently sparse in the domain represented by **G**, and the matrix $\mathbf{H}\mathbf{G}^{-1}$ satisfies the restricted isometry property (RIP) (*43*), CS techniques using l_1 based regularization can be used to estimate **w** from **u**, and then compute $\mathbf{v} = \mathbf{G}^{-1}\mathbf{w}$ to obtain an image. In our experiments, the image is already sparse in the spatial domain itself, so that **G** = **I** (where **I** is the identity matrix) is a sparse basis for our problem. For images that are not spatially sparse, bases such as the wavelet basis can be used to exploit sparsity, although we have not further explored this option. For the full 3D reconstruction shown in Fig. 6f, we made use of the sparsity of these two letters in water by applying the sparsity promoting basis pursuit de-noising (BPDN) algorithm. As can be seen, this prior knowledge about the image could be effectively exploited to improve image quality, significantly improving the dynamic range from 9 to 29 dB.

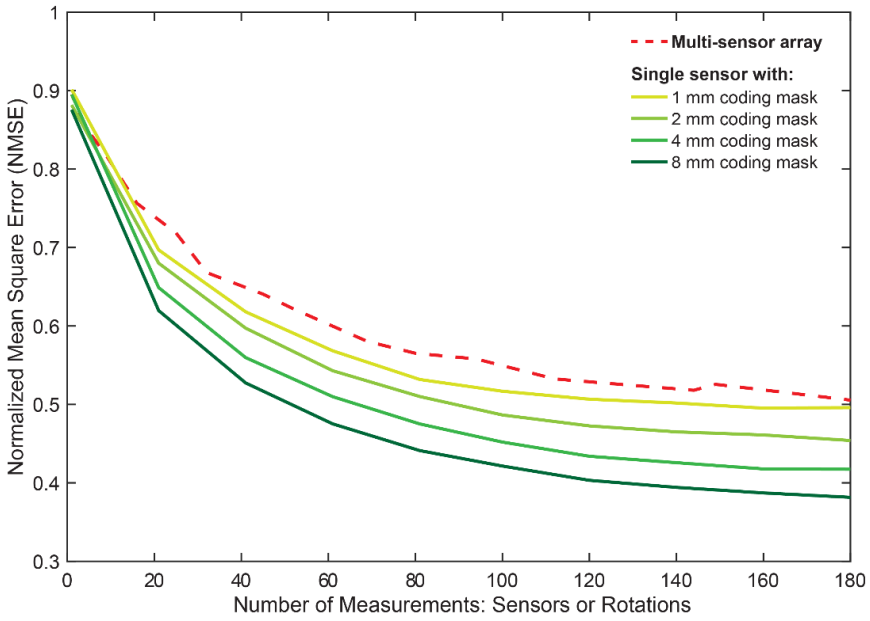

fig. S1. Imaging performance for a single sensor with coding mask and normal sensor arrays without coding mask. We computed a system matrix **H** for a normal array with varying sensor densities and for the proposed single sensor with coding mask with several thicknesses and varying rotations. A pre-defined image **v** (schematic drawing of a Toucan, in a xy-plane at a depth of 12.7 mm) was used to compute **u** via **u** = **Hv**. We then compared the estimated image $\hat{\mathbf{v}}$ with the true image **v** by computing the normalized mean square error. The results are shown above. A tradeoff in nmse between number of sensors in an array and number of rotations with a coding mask can be observed. By increasing the mask thickness more information is compressed in the measurement resulting in a better nmse for the same amount of measurements.

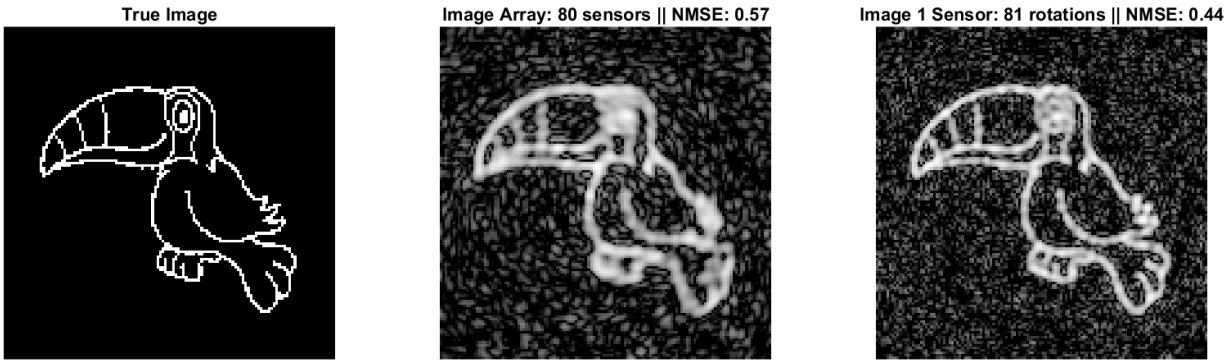

fig. S2. Image reconstruction example for a sensor array and a single sensor with coding mask for a comparable amount of measurements. Left panel shows the true image in a xy-plane at a depth of 12.7mm that was used to simulate the measurements for a normal array and single sensor with mask. Middle panel shows the reconstruction for an array with 80 sensors. The right panel shows the reconstruction for a single sensor with a 8 mm mask and 81 mask rotations.

Legends for movies S1 to S3

movie S1. A random delay coding mask breaks the phase uniformity of the ultrasound transmission to enable compressive imaging.

movie S2. Compressive 3D ultrasound imaging using a single sensor.

movie S3. Image reconstruction for a multisensor array and a single sensor with rotating coding mask.